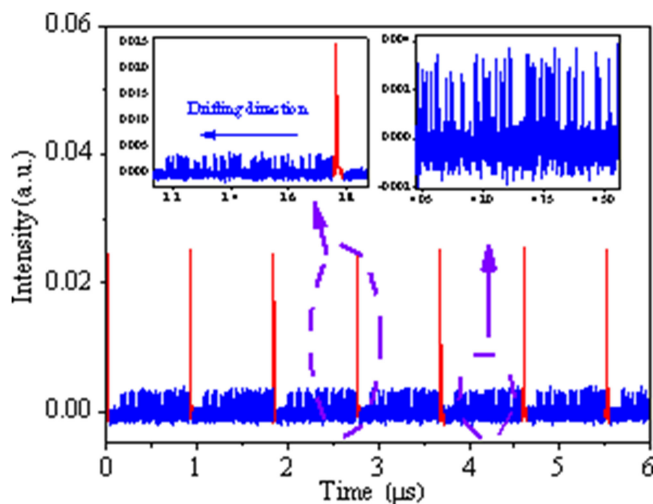


Evolution of Soliton Rain in a Tm-doped Passive Mode-Locked All-Fiber Laser



Volume 12, Number 4, August 2020

Feng Wang
Xin-lu Zhang
Jin-hui Cui
Jin-Jer Huang



DOI: 10.1109/JPHOT.2020.3012571

Evolution of Soliton Rain in a Tm-doped Passive Mode-Locked All-Fiber Laser

Feng Wang ¹, Xin-lu Zhang ², Jin-hui Cui,¹ and Jin-Jer Huang³

¹College of Physics and Optoelectronic Engineering, Harbin Engineering University, Harbin 150001, China

²School of Science, Heilongjiang University of Science and Technology, Harbin 150022, China

³School of Physics Science and Technology, Tiangong University, Tianjin 300387, China

DOI:10.1109/JPHOT.2020.3012571

This work is licensed under a Creative Commons Attribution 4.0 License. For more information, see <https://creativecommons.org/licenses/by/4.0/>

Manuscript received May 25, 2020; revised July 6, 2020; accepted July 24, 2020. Date of publication July 29, 2020; date of current version August 20, 2020. This work was supported in part by the National Natural Science Foundation of China under Grants 61775166 and 61275138, in part by the Nature Science Foundation of Tianjin under Grant 19JCZDJC32600, and in part by the Program for Innovative Research Team in the University of Tianjin under Grant TD13-5035. Corresponding author: Xinlu Zhang (e-mail: zhangxinlu1@aliyun.com).

Abstract: In this article, the numerical simulations and experimental investigations on the evolution of soliton rain in Tm-doped fiber laser were carried out, based on the nonlinear polarization rotation (NPR) technique. By carefully adjusting the polarization controller (PC) in the cavity, the soliton rain phenomenon was observed, in which the pulse train length of a drifting solitons was about 0.36 μs , 0.77 μs , and 0.92 μs , respectively. In order to further analyze the influence of PC on the formation of soliton rain, the corresponding numerical analysis was performed. The numerical simulation was in consistent with the experimental results. Our present research work was very meaningful to further investigate the nonlinear dynamics mechanisms of ultrafast fiber laser.

Index Terms: Fiber laser, Tm-doped, passive mode-locked, soliton rain.

1. Introduction

In the past two decades, much experimental research on passively mode-locked fiber laser has been done. It has received extensive attention as an ideal platform for studying new fields of soliton nonlinear dynamics [1]–[3]. Passive mode-locked fiber laser is caused by the interactions of nonlinear and dispersion effects, and these interactions produce many complex and interesting phenomena, such as dissipative soliton resonance [4], [5], soliton molecules [6], [7], harmonic mode-locking [8], [9] and soliton rain (SR) [10]–[13]. In 2009, S. Chouli and P. Grellu conducted an experimental study on SR [10], [11]. Since then, the internal mechanism of the nonlinear dynamics of soliton rain formation has been extensively studied. The SR phenomenon has also been discovered in other types of passively mode-locked fiber lasers, such as graphene/graphene oxide fiber lasers, nonlinear amplifying ring mirror fiber lasers, and nonlinear polarization rotating fiber lasers [12]–[16]. Recently, in a Yb-doped fiber laser with a standing wave cavity structure, P. Singh conducted experimental research on the SR state at lower pump power. It was found that the wavelength of the drifting soliton varies with the speed and direction of the drifting soliton [17]. In addition, K. Sulimany proposed that the noise-mediated pulse interaction mechanism could be used for numerical simulation. It was found that the formation of multi-soliton dynamic modes

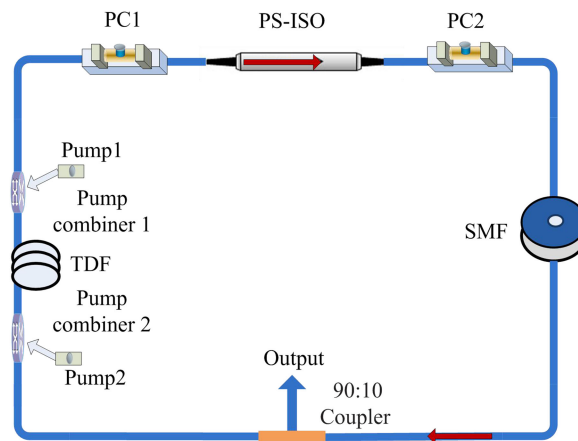


Fig. 1. Experimental setup of the passively mode-locked Tm-doped fiber laser.

in ultrafast lasers was mainly caused by Casimir-like remote interaction [18]. In addition, in the above-mentioned research, shorter cavities and lower pump power were used to form SR. In our present research, we have observed SR in the longer cavity. Due to the mechanism difference between the long cavity soliton interaction and the short cavity soliton interaction, the movement states of the drifting soliton are different. In a short cavity, there are multiple solitons with high repetition frequency and short separation (< 1 ps), and the interaction between solitons play the key role [19]. If the separation between solitons is larger than 1 ps, the long-distance interaction between solitons is achieved by dispersion waves [20]. This reflects that the separation between solitons is large in a long cavity, resulting in the very weak interaction among solitons [21].

In this paper, we have realized the pulse train length adjustment of a drifting soliton by adjusting a PC in a passive mode-locked Tm-doped fiber laser with large anomalous dispersion. The main factors affecting the drifting soliton train were analyzed by numerical simulation. Our present research is of great importance, and it builds a foundation for further analysis of the physical mechanism of soliton bunches formation and the nonlinear dynamic mechanism of SR.

2. Experimental Setup

The experimental setup of passively mode-locked Tm-doped fiber (TDF) laser based on nonlinear polarization rotation effect is presented in Fig. 1. The two pump sources possess a total maximum output power of 18 W and a central wavelength of 793 nm. The pump light was coupled into the cavity via two pump combiners (ITF, 793/2000 nm, Pump Channel 105/125, Signal Channel 10/130). A piece of single mode Tm-doped double-clad fiber (Nufern 10/130) with a length of 14 m is used as the gain medium, the TDF possesses an absorption coefficient of 3.0 dB/m at 793 nm. The group velocity dispersion (GVD) of the TDF is -91 ps²/km at 2000 nm. Two PCs are used to adjust the polarization state in the cavity. A polarization-sensitive isolator is used in the cavity to force the unidirectional operation of the ring cavity. The other fiber is the standard single mode fiber (SMF-28e) with a GVD parameter of -80 ps²/km. The Tm fiber laser has a ring cavity with a length of 183 m and the net cavity dispersion parameter is estimated to be -14.79 ps², which indicates that the Tm fiber laser operates at a large anomalous dispersion. The laser pulse is recorded by a 1 GHz bandwidth digital oscilloscope (Tektronix, MDO3104) and a fast InGaAs PIN photodetector (ET5000, EOT) with a rise time of 40 ps. The output spectra are measured by a monochromator (Omni- λ 300, Zolix) with a resolution of 0.1 nm and the InGaAs PIN photodetector. The radio frequency spectra are measured with the InGaAs PIN photodetector and an radio frequency (RF) signal analyzer (Rohde & Schwarz, FSV 40 GHz).

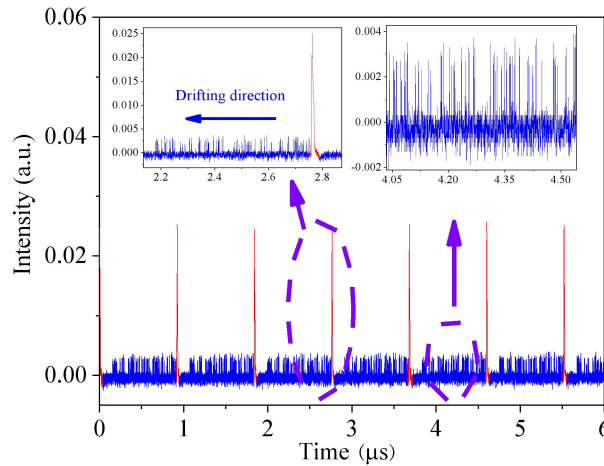


Fig. 2. SR state for a certain amount of round-trip periods. The SR state for a round-trip period is given in the left inset, and the inset on the right shows the enlarged drifting solitons.

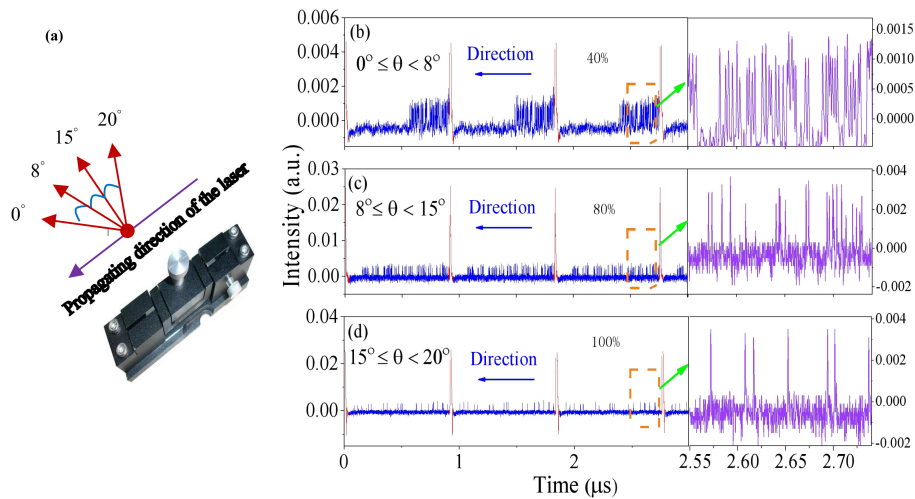


Fig. 3. (a) Diagram of the rotating angle for the rotating nut of PC. SR states for the rotating angles of (b) $0^\circ \leq \theta < 8^\circ$, (c) $8^\circ \leq \theta < 15^\circ$, and (d) $15^\circ \leq \theta < 20^\circ$.

3. Experimental Results and Discussion

When the total pump power reaches the mode-locking threshold of 5.4 W, the Tm fiber laser operates in a stable continuous wave (CW) mode-locking state. The SR state can be achieved by adjusting the PC setting, when the pump power is further increased to 6.14 W. Fig. 2 shows a typical SR state in which a series of dense drifting solitons are formed in the background noise and released from the condensed phase solitons. This process will be repeated periodically when there are no external disturbances. The left inset in Fig. 2 indicates the zooming-in of the marked portion of the main figure, and the condensed phase solitons and drifting solitons can be clearly seen. The right inset in Fig. 2 presents a large number of dense drifting solitons.

In the experiment, the polarization orientation in the cavity can be changed by adjusting the rotation angle θ of PC, so as to control the drifting solitons. Herein, a different rotation angle θ corresponds to a different laser output state. The rotation angle θ is given to be zero when the SR state begins to be formed, and the SR state can be kept for a rotating range of $0^\circ \sim 20^\circ$, as shown in Fig. 3. By fine-tuning the PC, the different number of drifting solitons may be found in the noise background. As shown in Fig. 3, the drifting solitons appear at different positions from the left to

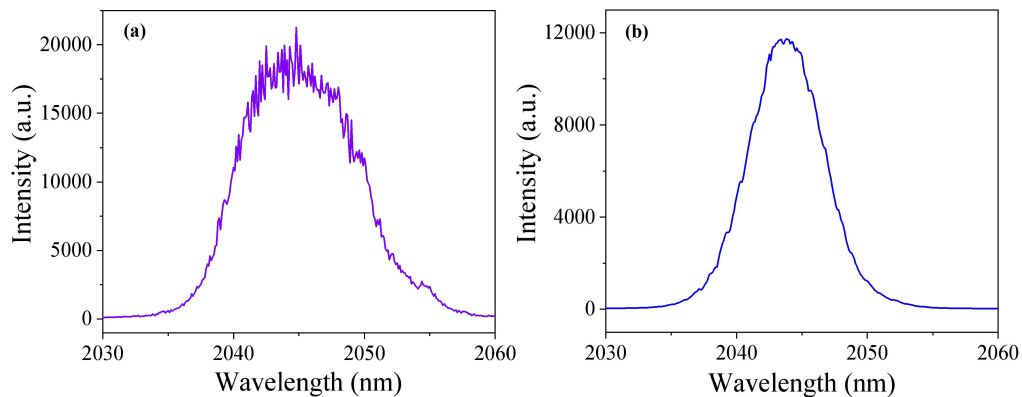


Fig. 4. (a) SR Spectrum for the rotating angle of $0^\circ \leq \theta < 20^\circ$, (b) CW mode-locked spectrum.

the right, and the drifting solitons occupy about 40%, 80%, and 100% of the background noise in a round-trip period. It can be seen in Fig. 3(b)–(d), SRs can be formed by adjusting PC in the range of $0^\circ \leq \theta < 8^\circ$, in which the drifting solitons occupy about 40% of the background noise in a round-trip period, which corresponds to a pulse train length of about $0.36 \mu\text{s}$. The intensity of drifting soliton is approximately 30% of that of the condensed phase soliton. In addition, the drifting solitons are formed at a fixed position periodically. SRs can also be formed in the range of $8^\circ \leq \theta < 15^\circ$, in which the drifting solitons occupy about 80% of the background noise in a round-trip period, which corresponds to a pulse train length of about $0.77 \mu\text{s}$. The intensity of drifting soliton is approximately 15% of that of the condensed phase soliton. In the range of $15^\circ \leq \theta < 20^\circ$, the drifting solitons occupy the entire background noise in a round-trip period, which corresponds to a pulse train length of about $0.92 \mu\text{s}$. The intensity of drifting soliton gradually reduces until it disappears, and the CW mode-locking state occurs. The right insets of Fig. 3(b)–(d) present a large number of dense drifting solitons, corresponding to the adjusting range of $0^\circ \leq \theta < 20^\circ$. For different adjusting range of PC, the occupy ratios and intensities of drifting solitons in the background noise are different. However, the repetition frequency of condensed phase soliton is always equal to the fundamental frequency of CW mode-locking, and the position and period of the condensed phase soliton remain unchanged. The adjustment of PC caused a phase delay difference, which changed the nonlinear loss of the cavity, thereby exciting drifting solitons of different train lengths.

The spectra of SRs in the range of $0^\circ \leq \theta < 20^\circ$ are shown in Fig. 4(a), while Fig. 4(b) shows the CW mode-locking spectrum. In comparison, it is found that the spectra of Fig. 4(a) have many sharp jitters. The irregular characteristics of the spectral sidebands indicated that the dynamic mechanism of drifting solitons was complex, which was the result of the interaction between different types of solitons. The directional movement of drifting solitons is mainly related to the following factors. First, the long-range interaction between the dispersive wave and the soliton wave caused resonance energy exchange, and the direction of energy flow depends on the relative phase [19], [22]. Second, the time domain of solitons was related to the phase delay difference in the cavity [23]. Third, special soliton bunches were formed under the action of strong pumping, in which the strong interaction between solitons can change their group velocities [11], [24]. Fourth, in the cavity, the unstable continuous wave component disturbs the background noise to produce drifting solitons [10], [11].

In order to further study the effect of polarization orientation on the SR in the cavity, we perform a numerical analysis for the SR. In the process of numerical simulation, the coupled Ginzburg-Landau equations (CGLEs) are used to describe the propagating of laser pulse in the fiber [25], [26].

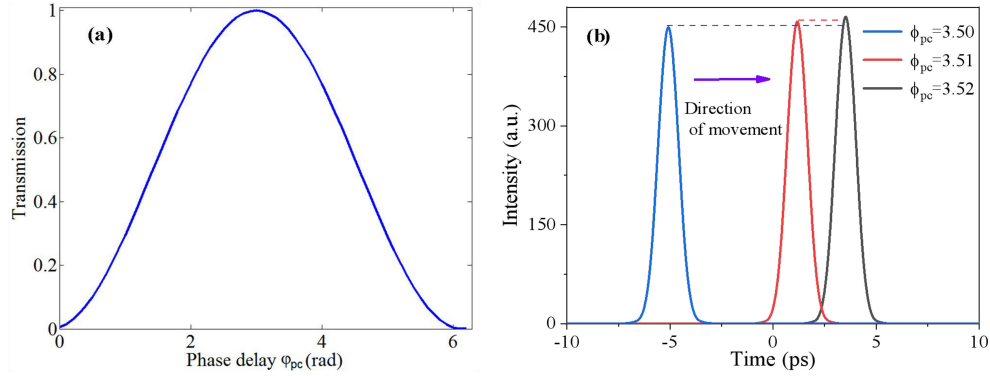


Fig. 5. Change of φ_{pc} caused by adjusting PC, (a) Relationship between the transmission function of the cavity and φ_{pc} , (b) Relationship between the time domain state of the single soliton pulse and φ_{pc} .

$$\frac{\partial u}{\partial z} = i\frac{\Delta\beta}{2}u - \delta\frac{\partial u}{\partial t} - i\frac{\beta_2}{2}\frac{\partial^2 u}{\partial t^2} + \frac{\beta_3}{6}\frac{\partial^3 u}{\partial t^3} + i\gamma\left(|u|^2 + \frac{2}{3}|v|^2\right)u + i\frac{\gamma}{3}v^2u^* + \frac{g}{2}u + \frac{g}{2\Omega_g^2}\frac{\partial^2 u}{\partial t^2} \quad (1)$$

$$\frac{\partial v}{\partial z} = -i\frac{\Delta\beta}{2}v + \delta\frac{\partial v}{\partial t} - i\frac{\beta_2}{2}\frac{\partial^2 v}{\partial t^2} + \frac{\beta_3}{6}\frac{\partial^3 v}{\partial t^3} + i\gamma\left(|v|^2 + \frac{2}{3}|u|^2\right)v + i\frac{\gamma}{3}u^2v^* + \frac{g}{2}v + \frac{g}{2\Omega_g^2}\frac{\partial^2 v}{\partial t^2} \quad (2)$$

In the above equations, u and v are the normalized envelopes of the optical pulses along the two orthogonal polarized modes of the optical fiber. $\Delta\beta = \beta_{0x} - \beta_{0y} = 2\pi B_m/\lambda$ is the wave-number difference between the two modes. $2\delta = 2\beta\lambda/2\pi c$ is the inverse group velocity difference. Ω_g is the gain bandwidth of the Tm-doped fiber laser. $g = g_0 \exp[-(|u|^2 + |v|^2)dt/E_{sat}]$ is the saturable gain coefficient of the Tm-doped fiber laser, wherein, g_0 is the small signal gain coefficient and E_{sat} is the gain saturation energy. The cavity used in the numerical simulation consists of the SMF with a length of 169 m, a thulium-doped fiber laser with a length of 14 m, a 10:90 output coupler with a 10% output, and an NPR mode locker. In order to conveniently compare the theoretical and experimental results, we used the following parameters: nonlinear fiber coefficients γ_{SMF} and γ_{TDF} are equal to $1.1 \text{ W}^{-1}\text{km}^{-1}$, and $3 \text{ W}^{-1}\text{km}^{-1}$ respectively, the GVD of TDF is $\beta'' = -91 \text{ ps}^2/\text{km}$ at 2000 nm, the SMF has a GVD of $\beta'' = -80 \text{ ps}^2/\text{km}$ at 2000 nm, the gain saturation energy E_{sat} is equal to 60 pJ, and the small-signal gain g_0 is 0.5 dB/m [27], [28]. The numerical simulation adopted the small signal gain mode, the Gaussian pulse width (10^{-13} s) and the pulse energy were given for initialization.

Adjusting PC can cause the phase delay to change in the cavity, which in turn changes the transmission function of the laser cavity, thereby achieving the control of the soliton state. The transmission function of the laser in the ring cavity is [26]:

$$T = \cos^2\alpha \cdot \cos^2\phi + \sin^2\alpha \cdot \sin^2\phi + \frac{1}{2}\sin 2\alpha \cdot \sin 2\phi \cdot \cos(\Delta\phi_F + \phi_{pc}) \quad (3)$$

where φ_{pc} is the cavity phase delay bias caused by the PC and $\Delta\phi_F$ is the phase delay resulting from the fiber including both the linear and nonlinear phase delay. α is the angle between the fast axis of the fiber and the axis of the polarizer, and ϕ is the angle between the fast axis of the fiber and the axis of the analyzer.

The simulation result of the relationship between transmission function and phase delay φ_{pc} was shown in Fig. 5(a). When $\alpha = 3.927$, $\phi = 0.785$, φ_{pc} is in the interval $[\pi, 2\pi]$, the laser is in the mode-locked state. After the energy of the soliton pulse reached a certain value, the pump power was further increased, the energy of the soliton pulse no longer increased, and the dispersion wave and background noise of a certain oscillation frequency would be amplified, thereby forming a new soliton pulse [26]. By solving Equations (1)–(3), the effect of the change in φ_{pc} on the evolution of the single soliton pulse was shown in Fig. 5(b). When φ_{pc} is 3.50, 3.51, 3.52, the state of the

soliton shifts, and the soliton peak and pulse energy change slightly. In the soliton rain state, a small adjustment of PC would cause φ_{PC} to change. Different φ_{PC} have different polarization states of the soliton, so the nonlinear loss is different. Because the condensed phase solitons have larger binding energy, the nonlinear loss has little effect on the condensed phase solitons, and the time domain position remains unchanged. However, the non-linear loss has a greater impact on the drifting soliton with smaller energy, which can directly cause the drifting soliton to flow in or flow out of the condensed phase soliton.

Based on the numerical simulation results, It was found that when certain conditions were satisfied in the cavity, the number of drifting solitons can be adjusted by increasing the gain energy or changing the angle α of the PC. As shown in Fig. 6(a), for $\alpha = 3.487$, drifting solitons may be formed at the position of -15.25 ps and disappear at the position of -59.82 ps. The pulse train length of drifting solitons between the two vertical white lines is 44.57 ps. In this case, the condensed phase soliton and the drifting solitons are coexisting states. According to the period of condensed phase soliton, one cycle period of condensed phase soliton in the cavity took about $0.92 \mu\text{s}$. It can be seen in Fig. 6(c) that when the laser was operated to the 700th round-trip period, a drifting soliton was formed in the range of -10 ps and -40 ps and the time corresponding to the peak was -23.74 ps. In the round-trip process of laser, drifting soliton moved further and further away from the condensed phase soliton due to the severe disturbance of dispersive waves and the spectral filtering effect. When the laser was operated to the 709th round-trip period, the soliton drifted to the range of -28 ps and -55 ps and the time corresponding to the peak was about -39.53 ps. In these 9 round-trip periods, the condensed phase soliton took about $8.235 \mu\text{s}$ and the relative movement time of drifting soliton peak was about 15.78 ps. We hypothesized that the speed of condensed phase soliton in the cavity was 3×10^8 m/s, so that the relative speed of drifting soliton can be gained, which was about 574.86 m/s. As indicated in Fig. 6(d), for $\alpha = 3.488$, drifting solitons can still be formed at the position of -15.25 ps and disappear at the position of -42.62 ps. The pulse train length of drifting soliton becomes short and is 27.37 ps. This means that by finely adjusting the PC, the pulse train length of drifting soliton can be changed, which is in consistent with our experimental results. As shown in Fig. 6(f), for $\alpha = 3.490$, the number of drifting solitons gradually decreases. When the round-trip period is greater than 600, the drifting solitons disappear, and only the stable condensed phase solitons are left. Fig. 6(b), (e) and (g) are the laser spectra, corresponding to Fig. 6(a), (d) and (f), respectively. It can be noted that there are obvious differences in Fig. 6(b), (e) and (g) near the central wavelengths. The round-trip periods from 500 to 1000 in Fig. 6(b) and (e) correspond to the coexisting states of the condensed phase soliton and the drifting soliton. Strong jitter appears near the center wavelength, which is similar to the experimental result, as shown in Fig. 4(a). When the round-trip period is from 600 to 1000 in Fig. 6(g), there is only condensed phase solitons left, the fluctuation near the spectral center wavelength is weak. It can be seen that, in the SR state, the spectra show complex and severe jitter features, indicating that there are complex interactions between the soliton wave and the dispersive wave [19]–[24]. In the simulation, when the continuous wave component and the amplified spontaneous emission (ASE) disturbance were not introduced, the soliton rain phenomenon was observed, which showed that the interaction between the dispersion wave and the soliton wave plays the key role in the directional movement of the drifting soliton. In our experiment, the peak intensity of condensed phase solitons was 2–5 times that of drifting solitons. In the simulation, the peak intensity of condensed phase solitons was 16 times that of drifting solitons. The comparison showed that the peak intensity of the drifting soliton in the experiment was significantly higher. This is because, in the experiment, there were continuous wave components and ASE in the cavity, and their mutual disturbance caused the drifting soliton peak and pulse energy to increase. When α (indicating polarization orientation) satisfies a certain condition, the dispersion wave in the laser cavity is not been sufficiently filtered, which results the strong interactions between the soliton wave and the dispersion wave, forming the SR. With the increasing of α , the pulse train length of drifting soliton is decreased, indicating that the intensity of dispersion wave can be adjusted by the polarization orientation in the cavity. The dynamic mechanism of directional movement of drifting soliton is: the interaction between the dispersive wave and soliton wave causes resonance energy exchange, and

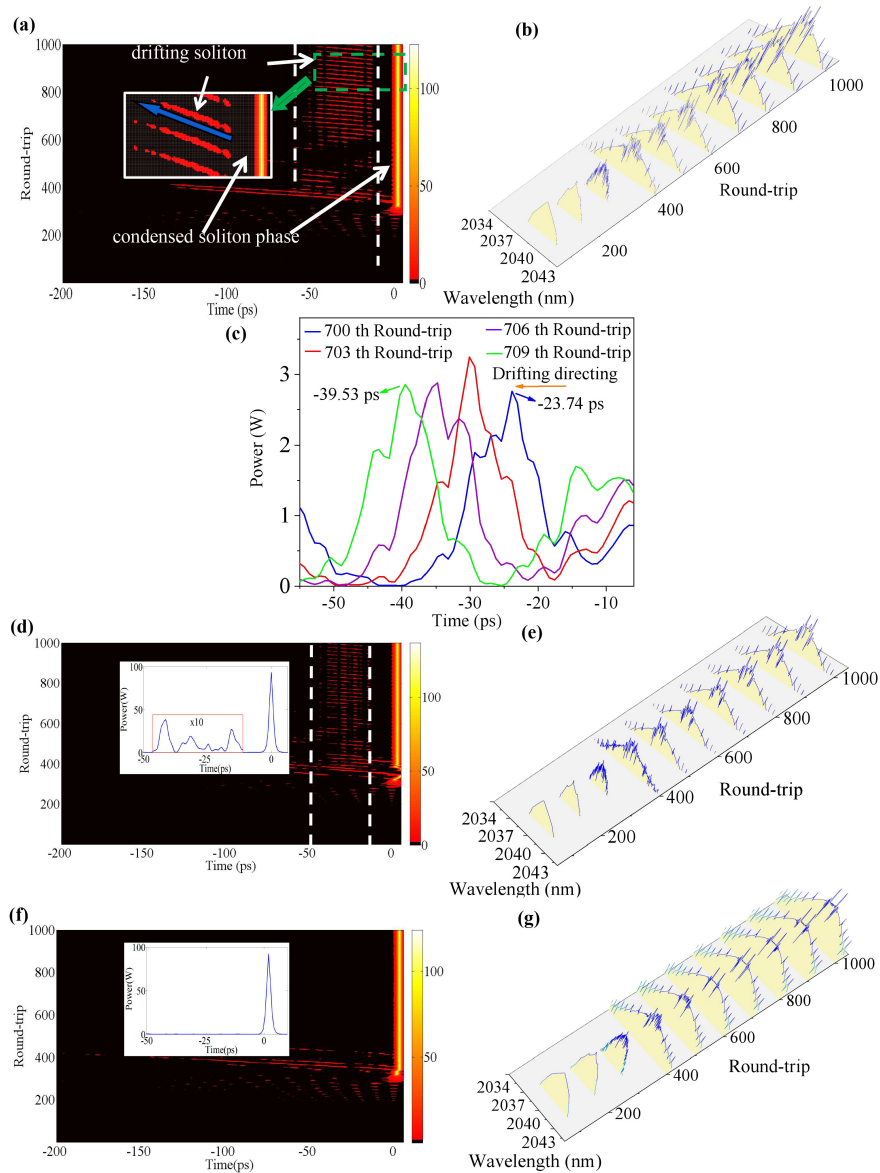


Fig. 6. SR states under certain conditions: (a) $\alpha = 3.487$, insets are the drifting soliton and the condensed phase in zoomed-in view (green rectangle area), where the blue arrow is the direction of the drifting soliton; (c) The motion state of drifting soliton was exhibited by choosing drifting soliton from the 700th to the 709th round-trip period in Fig. 5(a); (d) $\alpha = 3.488$ (the inset is pulse time domain diagram of the round-trip period 1000); and (f) $\alpha = 3.490$ (the inset is pulse time domain diagram of the round-trip period 1000). The corresponding optical spectra: (b) $\alpha = 3.487$, (e) $\alpha = 3.488$, and (g) $\alpha = 3.490$.

the direction of energy flow is the direction of movement of drifting soliton, which mainly depends on the relative phase.

4. Conclusion

In this article, the evolution of SR in a passively mode-locked Tm-doped all-fiber laser has been investigated theoretically and experimentally, and different multi-soliton dynamic modes are obtained. In the experiments, it is found that the evolution process of SR is very sensitive to the polarization

orientation of the laser and the spectra of SR have severe jitter, and the pulse train length of the drifting soliton can be adjusted by changing the parameters of PC. In addition, the evolution of SR state has been theoretically analyzed by using the Ginzburg-Landau equations, and the numerical results are in consistent with the experimental results.

Acknowledgment

The authors would like to thank the anonymous reviewers for their valuable suggestions.

References

- [1] M. E. Fermann, and I. Hartl, "Ultrafast fibre lasers," *Nat. Protoc.*, vol. 7, no. 11, pp. 868–874, 2013.
- [2] Y. Song, X. Shi, C. Wu, D. Tang, and H. Zhang, "Recent progress of study on optical solitons in fiber lasers," *Appl. Phys. Rev.*, vol. 6, no. 2, pp. 021313–021333, 2019.
- [3] H. Zhang, D. Y. Tang, L. Zhao, and N. Xiang, "Coherent energy exchange between components of a vector soliton in fiber lasers," *Opt. Express*, vol. 16, no. 17, pp. 12618–12623, 2008.
- [4] W. Chang, A. Ankiewicz, J. Soto-Crespo, and N. Akhmediev, "Dissipative soliton resonances," *Phys. Rev. A.*, vol. 78, no. 2, pp. 023830–023839, 2008.
- [5] P. Grelu, W. Chang, A. Ankiewicz, J. M. Soto-Crespo, and N. Akhmediev, "Dissipative soliton resonance as a guideline for high-energy pulse laser oscillators," *J. Opt. Soc. Am. B.*, vol. 27, no. 11, pp. 2336–2341, 2010.
- [6] P. Grelu, and J. Soto-Crespo, "Temporal soliton "molecules" in mode-locked lasers: Collisions, pulsations, and vibrations," *Dissipative solitons: From optics to biology and medicine*, pp. 1–37, Springer, 2008.
- [7] Y. Q. Huang, Z. A. Hu, H. Cui, Z. C. Luo, A. P. Luo, and W. C. Xu, "Coexistence of harmonic soliton molecules and rectangular noise-like pulses in a figure-eight fiber laser," *Opt. Lett.*, vol. 41, no. 17, pp. 4056–4059, 2016.
- [8] G. Sobon, J. Sotor, and K. M. Abramski, "Passive harmonic mode-locking in Er-doped fiber laser based on graphene saturable absorber with repetition rates scalable to 2.22 GHz," *Appl. Phys. Lett.*, vol. 100, no. 16, pp. 161109–161113, 2012.
- [9] C. Lecaplain, and P. Grelu, "Multi-gigahertz repetition-rate-selectable passive harmonic mode locking of a fiber laser," *Opt. Express*, vol. 21, no. 9, pp. 10897–10902, 2013.
- [10] S. Chouli, and P. Grelu, "Rains of solitons in a fiber laser," *Opt. Express*, vol. 17, no. 14, pp. 11776–11781, 2009.
- [11] S. Chouli, and P. Grelu, "Soliton rains in a fiber laser: An experimental study," *Phys. Rev. A.*, vol. 81, no. 6, pp. 063829–063839, 2010.
- [12] C. Bao, X. Xiao, and C. Yang, "Soliton rains in a normal dispersion fiber laser with dual-filter," *Opt. Lett.*, vol. 38, no. 11, pp. 1875–1877, 2013.
- [13] Q. Y. Ning *et al.*, "Vector nature of multi-soliton patterns in a passively mode-locked figure-eight fiber laser," *Opt. Express*, vol. 22, no. 10, pp. 11900–11911, 2014.
- [14] Y. F. Song, L. Li, H. Zhang, D. Y. Tang, and K. P. Loh, "Vector multi-soliton operation and interaction in a graphene mode-locked fiber laser," *Opt. Express*, vol. 21, no. 8, pp. 10010–10018, 2013.
- [15] Y. Meng, S. Zhang, X. Li, H. Li, J. Du, and Y. Hao, "Multiple-soliton dynamic patterns in a graphene mode-locked fiber laser," *Opt. Express*, vol. 20, no. 6, pp. 6685–6692, 2012.
- [16] A. Niang, F. Amrani, M. Salhi, P. Grelu, and F. Sanchez, "Rains of solitons in a figure-of-eight passively mode-locked fiber laser," *Appl. Phys. B.*, vol. 116, no. 3, pp. 771–775, 2014.
- [17] C. Singh *et al.*, "Experimental study on soliton rain patterns in Yb-doped all-fiber standing wave cavity configuration," *IEEE Photon. Technol. Lett.*, vol. 28, no. 14, pp. 1533–1536, 2016.
- [18] K. Sulimany *et al.*, "Bidirectional soliton rain dynamics induced by casimir-like interactions in a graphene mode-locked fiber laser," *Phys. Rev. Lett.*, vol. 121, no. 13, pp. 133902–133908, 2018.
- [19] D. Y. Tang, B. Zhao, L. M. Zhao, and H. Y. Tam, "Soliton interaction in a fiber ring laser," *Phys. Rev. E*, vol. 72, no. 1, 2005, Art. no. 016616.
- [20] P. Grelu, F. Belhache, F. Gутty, and J. M. Soto-Crespo, "Phase-locked soliton pairs in a stretched-pulse fiber laser," *Opt. Lett.*, vol. 27, no. 11, pp. 966–968, 2002.
- [21] J. K. Jang, M. Erkintalo, S. G. Murdoch, and S. Coen, "Ultraweak long-range interactions of solitons observed over astronomical distances," *Nat. Photon.*, vol. 7, no. 8, p. 657, 2013.
- [22] L. N. Duan, X. M. Liu, and L. R. Wang, "Comparison of pulse evolutions in low and ultra-large anomalous dispersion mode-locked fiber lasers," *Laser Phys.*, vol. 21, no. 5, pp. 948–953, 2011.
- [23] X. Liu, "Interaction and motion of solitons in passively-mode-locked fiber lasers," *Phys. Rev. A*, vol. 84, no. 5, 2011, Art. no. 053828.
- [24] P. Grelu, and N. Akhmediev, "Group interactions of dissipative solitons in a laser cavity: The case of $2 + 1$," *Opt. Express*, vol. 12, no. 14, pp. 3184–3189, 2004.
- [25] D. Y. Tang, L. Zhao, and B. Zhao, "Soliton collapse and bunched noise-like pulse generation in a passively mode-locked fiber ring laser," *Opt. Express*, vol. 13, no. 7, pp. 2289–2294, 2005.
- [26] D. Tang, L. M. Zhao, B. Zhao, and A. Liu, "Mechanism of multisoliton formation and soliton energy quantization in passively mode-locked fiber lasers," *Phys. Rev. A*, vol. 72, no. 4, pp. 043816–043854, 2005.
- [27] H. Xia, H. Li, X. Zhang, S. Zhang, X. Tang, and Y. Liu, "Characteristics of dissipative solitons in an all-fiber thulium-doped fiber ring laser," *Opt. Eng.*, vol. 52, no. 5, 2013, Art. no. 054201.
- [28] X. Wu *et al.*, "Tunable all-optical actively mode-locked fiber laser at 2 μm based on tellurite photonic crystal fiber," *Laser Phys. Lett.*, vol. 15, no. 6, 2018, Art. no. 065103.